buildings

MDPI

Article

An Experimental Study on Plate Splicing of Prefabricated Plate Foundation

Wenming Wang [1,2,†], Yahui Gao [1,2,†], Zhen Wang [1,2,*], Lijuan Zhang [3], Zhonghai An [3] and Sicheng Shao [4]

1 School of Civil Engineering, Shandong Jianzhu University, Jinan 250101, China; wangwenmingmr@sdjzu.edu.cn (W.W.); gaoyahui1212@126.com (Y.G.)
2 Key Laboratory of Building Structural Retrofitting & Underground Space Engineering, Ministry of Education, Shandong Jianzhu University, Jinan 250101, China
3 Shandong Electric Power Engineering Consulting Institute Corporation Limited, Jinan 250013, China; zhanglijuan@sdepci.com (L.Z.); anzhonghai@sdepci.com (Z.A.)
4 Citic Construction Corporation Limited, Beijing 100027, China; shaosc@citic.com
* Correspondence: zhenwang25@126.com
† These authors contributed equally to this work.

Abstract: Tower foundations are generally of a cast-in-place structure with the disadvantages of low industrialization level and long construction period. The development of prefabricated foundation for transmission line projects is efficient to improve the industrialization level of the construction of tower foundation. In this study, the schemes of post-pouring belt U-shaped steel connection, post-pouring belt lap connection, grouting sleeve connection, and post-tensioned bond prestressed reinforcement connection, which have been widely used on building structures, are newly proposed to apply on plate foundation. The schemes were compared on processing, transporting, on-site constructing and performance. The pseudo-static tests on cast-in-place plate strip, post-pouring belt U-shaped steel connection and post-pouring belt lap connection plate strip were carried out. The results revealed that all the test plate bands were damaged in the bending mode, same as that of ordinary concrete. When U-shaped steel is adopted, more than 90% of the cast-in-place bearing capacity can be reached. The initial stiffness of prefabricated plate strip and cast-in-place strip is basically the same. The load-bearing capacity of the component is relevant to the anchorage length of the U-shaped steel. Although increasing the concrete strength of post-cast belt can improve the ultimate bearing capacity and shorten the construction period, the deformation capacity is reduced. Compared to other connection methods, post-pouring belt U-shaped steel connections have the advantage of simple construction, higher bearing capacity and stability. In summary, the post-pouring belt U-shaped steel connection scheme is recommended.

Keywords: prefabricated construction; plate foundation; bending performance; quasi-static test; transmission line

Citation: Wang, W.; Gao, Y.; Wang, Z.; Zhang, L.; An, Z.; Shao, S. An Experimental Study on Plate Splicing of Prefabricated Plate Foundation. *Buildings* **2023**, *13*, 2114. https://doi.org/10.3390/buildings13082114

Academic Editor: Harry Far

Received: 25 July 2023
Revised: 15 August 2023
Accepted: 17 August 2023
Published: 21 August 2023

1. Introduction

Due to the extremely rapid development of economy, power energy has been increasingly demanded in recent decades. A large number of transmission line projects have been designed to meet the developing requirements. Tower foundation is an important part of transmission line, including plate foundation, pile foundation, and rock bolt foundation, generally cast at the site. The traditional construction process requires a large investment, a long construction period, excessive labor demand, and great construction difficulty in complex geological environments. Therefore, technical development is strongly desired.

Currently, extensive studies focus on the mechanical performances and properties of transmission tower foundation, while the prefabricated structure design and construction of transmission tower foundation have been barely explored, hindering transmission tower lines developing to reach modernization and high technology [1–4]. Li Wei and his team paid attention to the transmission tower found in saline areas, and they explored the utilization of ultra-high-performance concrete (UHPC) to replace traditional concrete to improve durable proprieties [5]. Guanglin Yuan et al. [6] prompted a new design of hybrid plate foundations, which verified a good resistance to deformation and stress within the system. Zhou Yingbo et al. [7] evaluated the stability of a 500 kV transmission tower foundation on the landslide. As a result, merely the wind speed and buried depth of the tower were attributed [7]. Nevertheless, prefabricated technology on transmission tower foundations, having the advantages of high engineering quality, fast construction speed, environmental friendliness, ease of construction, low site management, and low labor costs, is scarcely studied.

Regarding prefabricated structures and construction, the connection of components is critical to ensure its workability. Some prefabricated structure connection methods are shown in Table 1. Moreover, a strong connection can improve the mechanical behavior and seismic resilience of the nodes [8–14]. Studies based on prefabricated building structures have been widely reported. Abtin Baghdadi et al. [15] proposed new types of connection by changing its geometric shape for precast concrete structures, which can achieve 85% of the strength of the whole structure. Chen Yihu et al. [16] investigated the mechanical properties of U-shaped steel ring-buckle connections in prefabricated concrete beam–column nodes, proving that ring-buckle steel in beam–column nodes can effectively transfer the tensile and compressive forces required for connection, ensuring the safety of the connection. Linfeng Lu et al. [17] investigated a novel prefabricated concrete composite slab, which adopts the high-strength bolt as the shear connector. The composite slabs showed good bending bearing capacity and ductility. Liu Xue-chun et al. [18] investigated a prefabricated steel-reinforced concrete slab with a C-type steel border, which can effectively improve the connection strength and increase the rigidity of the floor. However, the force pattern and construction characteristics of transmission tower plate foundations are completely different from ordinary building structures. The connection method and design of the prefabricated plate foundation of the transmission tower need to be studied.

Table 1. Prefabricated structure connection method.

Year	Structure	Connection Method
2019	beam–column	U-type reinforcement
2022	beam–column	Replaceable steel plate damper
2022	continuous rigid-frame bridge	Grouting Sleeve Connection
2022	slab	High-strength bolt
2022	slab	C-type steel border
2023	walls	Welded joint

In this study, a variety of prefabricated schemes are proposed for plate foundations widely used in the field of a transmission towers in order to improve green and intelligent construction technology on tower foundations, shorten construction time, and reduce the labor force. Subsequently, different connection methods in terms of component processing and site construction are compared. A quasi-static experimental study was carried out on a cast-in-place plate, post-cast U-shaped steel plate connection, post-cast lap plate connection, and reinforcement sleeve plate connection, respectively, to investigate the force performance of the connection between independent plates. The load-bearing capacity and failure patterns are recorded and analyzed. Furthermore, numerical analysis is conducted to compare the displacement and stress distribution between the schemes of cast-in-place plate and post-cast U-shaped steel plate connection.

2. Prefabricated Schemes of Plate Foundation

The plate foundation of slope type widely used in transmission line engineering is as shown in Figure 1. The buried depth is generally 3–5 m. The width of the base plate is generally above 3 m. Due to the large size, transportation and hoisting of a complete plate foundation are extremely difficult. In the current study, plate foundation is distributed into blocks for prefabrication, as shown in Figure 1a. Two parallel splits are set vertical to reinforcing bars; thus, the plate foundation is separated into three blocks. The main column is subsequently connected to the foundation by grouted sleeves on site. Four prefabrication schemes are proposed: reinforcement sleeve plate connection, post-tensioned bonded prestressing tendon connections, post-cast U-shaped steel plate connection, and post-cast lap plate connection. The characters of each scheme are listed and compared in Table 2.

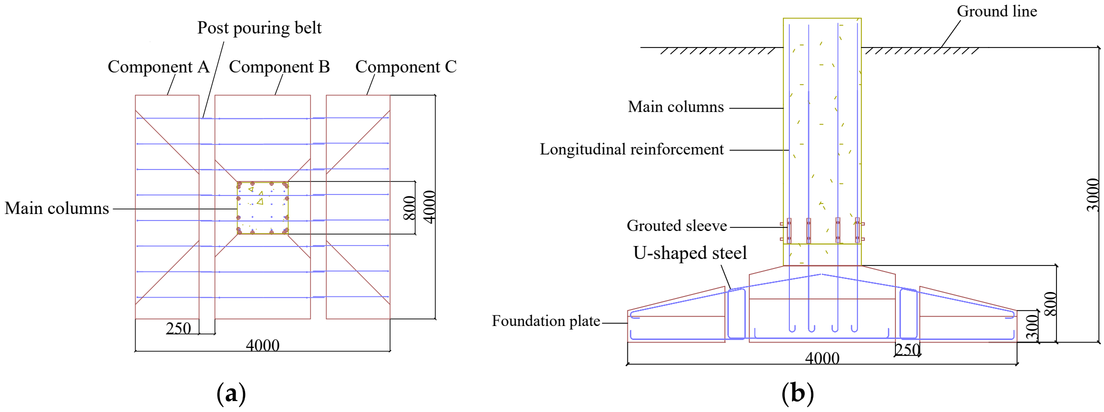

Figure 1. Plate Foundation. (**a**) Top View (**b**) Front View.

Table 2. Characters of Each Scheme.

Connection Modes	Processing Difficulty	Transportation Difficulty	Hoisting Difficulty	Other (Effects)
Post-cast strip U-shaped steel connection (recommended scheme)	low	low	low	Low volume poured on site; some steel wasted.
Post-pouring strip lap connection	low	low	low	Steel saving; large width of post-cast strip; less reliable.
Grouting sleeve connection	medium	low	high	High connection reliability. high grouting difficulty; difficult horizontal alignment on site; poor economy.
Post-tensioning connection with bonded prestressed reinforcement	medium	low	low	Slow crack development; high inter-plate bond strength; full use of steel strength; improved foundation stressing properties. Difficult to process; difficult to construct on site; large foundation excavation.

The construction methods and technical effects of each scheme are as follows.

① Post-cast U-shaped steel plate connection

U-shaped steel is partially exposed outside the plate strip, as shown in Figure 2. After being hoisted in place at the construction site, the concrete to connect Component 1 and Component 2 are cast. The use of U-shaped steel connections can reduce the anchorage length of the reinforcement to 0.6 *la* [19]. The width of the post-cast strip zone can be further reduced by reducing the diameter of the steel or increasing the strength of post-cast strip zone material. Thus, the quantity of concrete to be cast on site can be decreased. This scheme is highly recommended in this study.

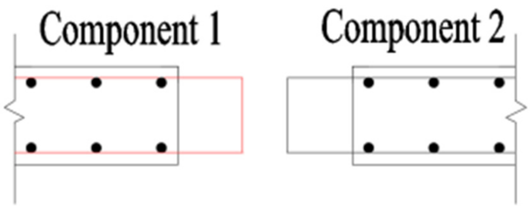

Figure 2. Post-cast U-shaped Steel Plate Connection.

② Post-cast lap plate connection

The stressed steel is exposed outside the plate strip, as shown in Figure 3. After being hoisted in place at the construction site, the concrete is poured for connecting Component 1 and Component 2. Compared with the U-shaped steel connection mode, this mode is able to save more steel.

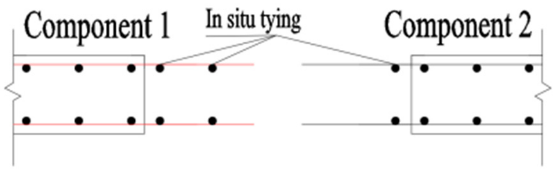

Figure 3. Post-cast Lap Plate Connection.

③ Grouting Sleeve Connection

The upper and lower bars of the bottom plate are embedded with steel sleeves, as shown in Figure 4. Grouting is carried out after the constructing elements are hoisted. On the premise of a good quality of grouting, the grouting sleeve connection can be achieved with high reliability.

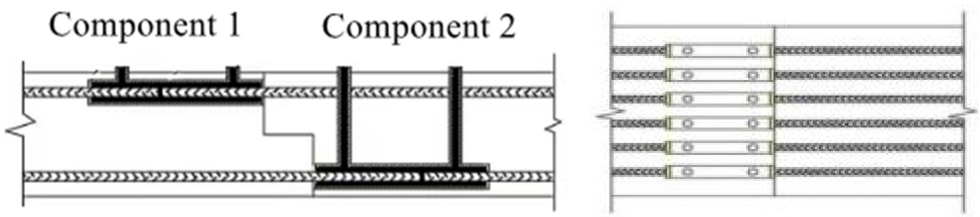

Figure 4. Grouting Sleeve Connection.

④ Post-tensioning Connection with Bonded Prestressed Reinforcement

Each component buries the bellows along the vertical seam direction, as shown in Figure 5. After excavation of the foundation pit, the components are hoisted into position. The threading, tensioning, and grouting of the reinforcement are completed in the foundation pit. The use of prestressing techniques can effectively slow down the development of cracks in the bottom plate, providing significant advantages in corrosive geological conditions [20,21]. This connection method significantly improves the bond strength between plates. Steel reinforcements can be fully applied for strength bearing. The stress state of concrete is optimized, which in turn improves the mechanical properties of the foundation.

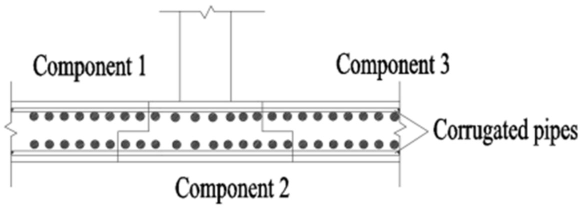

Figure 5. Post-tensioning Connection with Bonded Prestressed Reinforcement.

The post-tensioned bonded prestressing tendon connection solution is difficult to process, as bellows are required for processing the prefabricated elements. Additional reinforcement tensioning and bellow grouting operations were added to the construction site, resulting in a cumbersome construction process. During the construction process, additional pit excavation is required due to increased work surface. The post-tensioned bonded prestressing tendon connection solution is not recommended given the economic waste and the difficulty of lifting on site.

The adoption of a direct lap scheme leads to an increment in the width of post-pouring zone. The reliability of the connection mode is low. Nevertheless, compared with the U-shaped steel connection scheme, this scheme consumes less reinforcement steel. For the base plate, it is difficult to complete the horizontal docking and hoist on-site when using the grouted sleeve connection scheme. However, grouted sleeve connections are currently a widely used connection method with reliable connection strength. In summary, three schemes of U-shaped steel connection, lap connection of reinforcement, and grouted sleeve connection are identified for the plate connection test. The reliability of the different connection methods is verified to provide a reference for practical engineering applications.

3. Method and Material

3.1. Test Design

In this study, 9 specimens of foundation plate strips were designed and processed. The parameters are shown in Table 3. The concrete adopts the way of on-site preparation and is prepared according to C30. U-shaped steel lap lengths are taken as 0.3 *la*, 0.4 *la* and 0.6 *la*, respectively. The *la* value is calculated according to the reinforcement anchorage length calculation formula, as shown in Formula (1):

$$la = \alpha \frac{f_y}{f_t} d. \tag{1}$$

Table 3. Parameters of Specimens.

Specimen Number	Assembly Planning	Member Size/mm × mm × mm	Splice Length	Material of Panel Zone	Steel Bar Types
1-1	Cast-in-Place	1700 × 400 × 300	/	/	HPB300
2-1	U-shaped steel connection		0.3 *la*	C30	
2-2	U-shaped steel connection		0.4 *la*	C30	
2-3	U-shaped steel connection		0.6 *la*	C30	
2-4	U-shaped steel connection		0.3 *la*	High strength grouting material	
2-5	U-shaped steel connection		0.6 *la*	C30	
2-6	100 MPa U-shaped steel connection		0.6 *la*	C30	
3-1	Lap connections		*la*	C30	
4-1	Grouted Sleeve Connection		/	High-strength grouting material	

α is the form factor of anchoring reinforcement that takes the value of 0.16 according to the Code for the Design of Concrete Structures [22]. f_y is the design value of tensile strength of common reinforcement. f_t is the design value of axial tensile strength of concrete. d is the diameter of anchoring reinforcement.

The geometric dimensions and reinforcement of test piece 1-1 are shown in Figure 6.

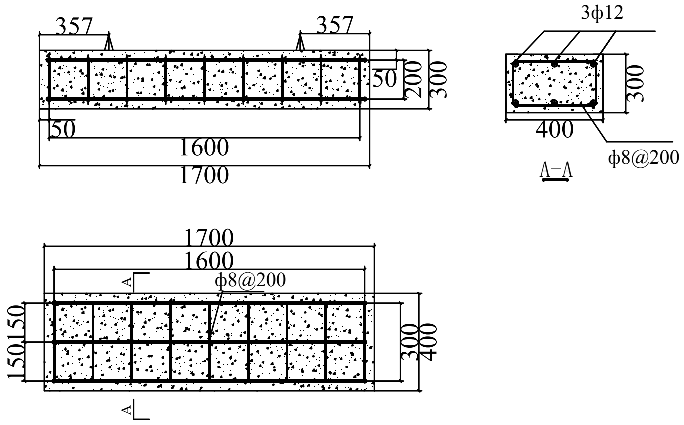

Figure 6. Dimension and Rebar Arrangement of Specimen 1-1.

Geometric dimension and reinforcement of Specimens 2-1, 2-2, and 2-3 are shown in Figure 7. The field machining diagram is shown in Figure 8. After each component is cured for 28 days, 4 reinforcing bars parallel to the split direction are added at the 4 corners of the U-shaped steel. Subsequently, the concrete is poured at the splicing site to complete the component connection.

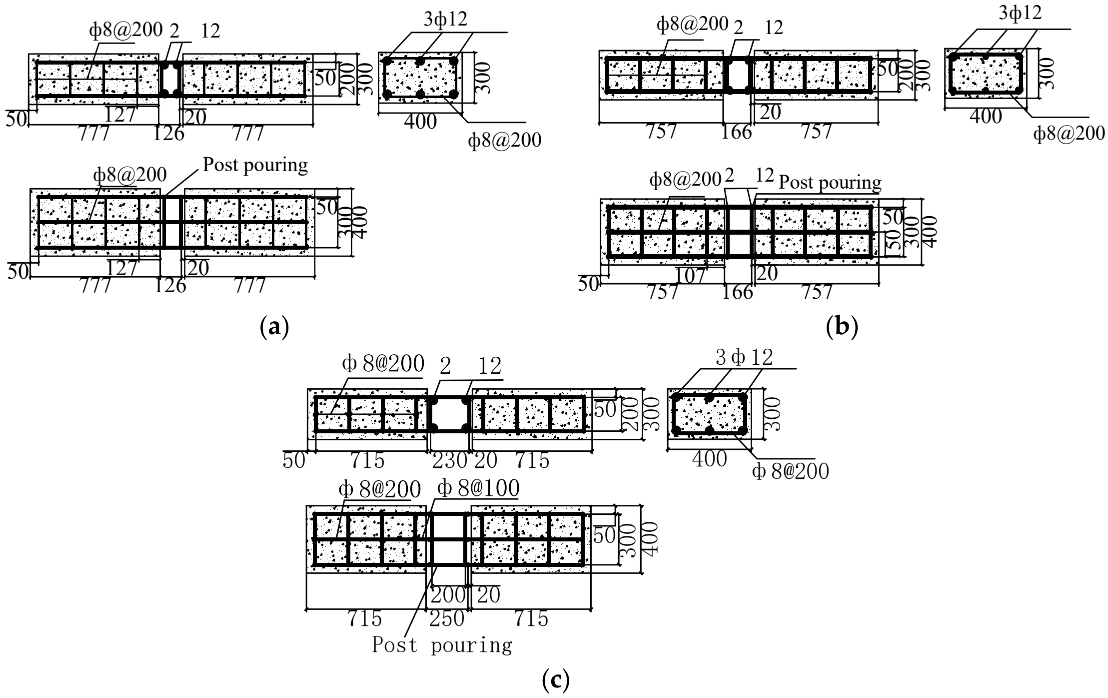

Figure 7. Dimensions and Rebar Arrangement of Post-pouring Belt U-shaped steel Connection. (**a**) Specimen 2-1; (**b**) Specimen 2-2; (**c**) Specimen 2-3.

Figure 8. Field Processing Diagram of Post-pouring Belt U-shaped steel Connection. (**a**) Specimen 2-1; (**b**) Specimen 2-2; (**c**) Specimen 2-3.

Upper and lower layers of reinforcement in Specimen 3-1 are independent. The lap part is arranged with stirrup to ensure that no shear failure occurs in the post-cast section. The geometric dimension and reinforcement of Specimen 3-1 are shown in Figure 9. The field machining diagram is shown in Figure 10. In Specimen 4-1, one member has an embedded grouting sleeve. The exposed length of the other member reinforcement should be greater than 8d in order to ensure full insertion into the sleeve. Splicing and grouting are carried out after the two components are processed. Grouting material should meet the requirements of relevant regulations. Geometric dimension and construction are shown in Figure 11. The field machining diagram is shown in Figure 12.

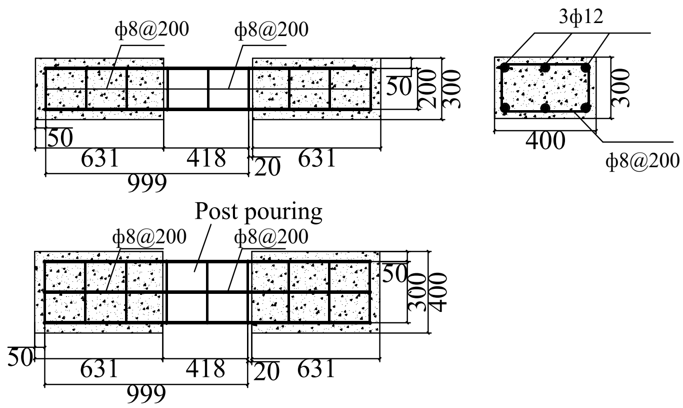

Figure 9. Dimensions and Rebar Arrangement of Specimen 3-1.

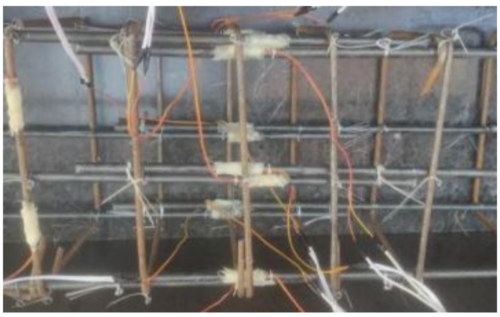

Figure 10. Field machining diagram of Specimen 3-1.

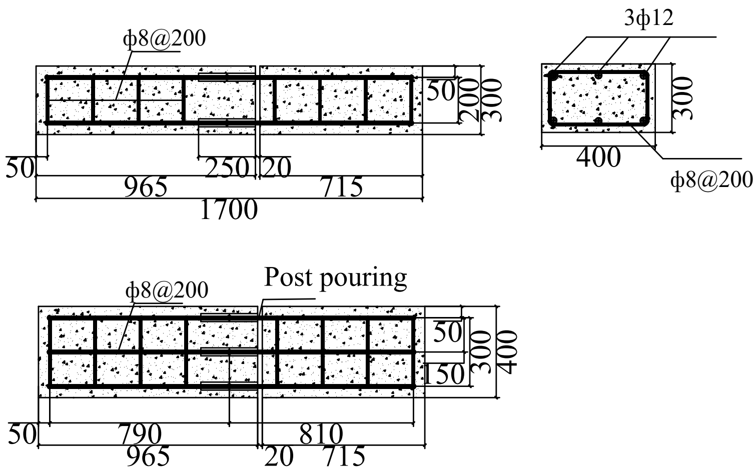

Figure 11. Dimensions and Rebar Arrangement of Specimen 4-1.

Figure 12. Field machining diagram of Specimen 4-1.

3.2. Material Properties

HPB300 is utilized for the longitudinal reinforcement and stirrup in the test, with the diameters of 12 mm and 8 mm, respectively. Each type of reinforcement is sampled by the "Standard for Test Methods of Concrete Structures" (GB/T 50152-2012) [23]. The reinforcement strength is then obtained by tensile testing. The test device is shown in Figure 13. The stress–strain curve of the longitudinal reinforcement is shown in Figure 14. Its mechanical properties are shown in Table 4.

Figure 13. Device for Rebar Tensile Test.

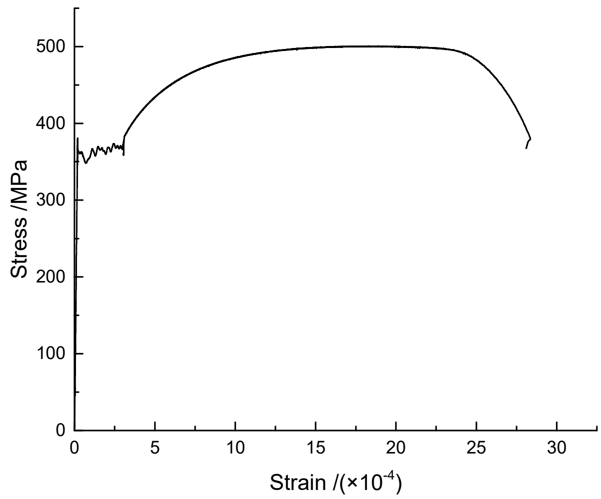

Figure 14. The stress–strain curve of the longitudinal rebar.

Table 4. Mechanical Properties of Rebars.

Bar Diameter (mm)	Yield Strength (MPa)	Ultimate Strength (MPa)	Elastic Modulus (MPa)	Elongation after Fracture (%)
8	435.2	588.3	2.01×10^5	20.27%
12	378.4	494.7	2.05×10^5	27.65%

The concrete test blocks for the first pouring part and the post-pouring part need to be reserved. When conducting material tests, the load is applied continuously and uniformly at a rate of 0.5 MPa per second. According to the "Standard for test method of mechanical properties on ordinary concrete" (GB/T50081-2002) [24], the value of compressive strength of concrete cube is measured. The compressive strength of a non-standard size specimen of $100 \times 100 \times 100$ is multiplied by the size conversion coefficient of 0.95. The material property test results are shown in Table 5. The maximum value of the strength measurement of the three post-cast material specimens differs from the middle value by more than 15%. Thus, the maximum value and the minimum value are excluded, and the middle value is taken as the compressive strength value of the specimen. The temperature and humidity are higher after the first part of the pour, which is more conducive to the growth of concrete strength than in the post-poured part.

Table 5. Cube Compressive Strength of Concrete.

Specimen Type	Test Piece 1 f_{cu} (Mpa)	Test Piece 2 f_{cu} (MPa)	Test Piece 3 f_{cu} (MPa)	Compressive Strength f_{cu} (MPa)	Axial Compressive Strength f_c (MPa)
Pre-cast part	43.5	40.2	43.9	42.5	32.29
Post-cast part	34.8	28.9	28.2	28.9	21.96

The compressive and bending strengths of high-strength grout were tested using 40 mm × 40 mm × 160 mm specimens. Three specimens were made for each group and left to be molded after 24 h. The compressive strength test was carried out after 28 days of standard maintenance. The flexural test was loaded on the cement flexural strength testing machine at a loading rate of 50.0 N/s. The compressive test was loaded on a pressure testing machine with a stress-controlled loading rate of 0.5 MPa/s. The strength of the high-strength grout is shown in Table 6.

Table 6. Strength of high-strength grouting material.

Specimen Type	Compressive Strength (MPa)	Bending Strength (MPa)
High-strength grouting material	75.4	10.1

3.3. Test Loading Method and Measurement Method

The prefabricated plate foundation plate strip is loaded using a 1000 kN testing machine at the Structural Testing Laboratory of Shandong Jianzhu University. A single-point centralized loading mode in the mid-span is used. The pre-load is conducted before the formal loading. After the measuring equipment works normally and the load, displacement, and strain data are stable, the material is unmounted to the initial state to start formal loading. The test load is applied in 5 kN increments and remains constant for 5 min after each applied load is stabilized. A movable hinge support and a fixed hinge support are used to achieve simple support boundary conditions. The test loading device is shown in Figure 15.

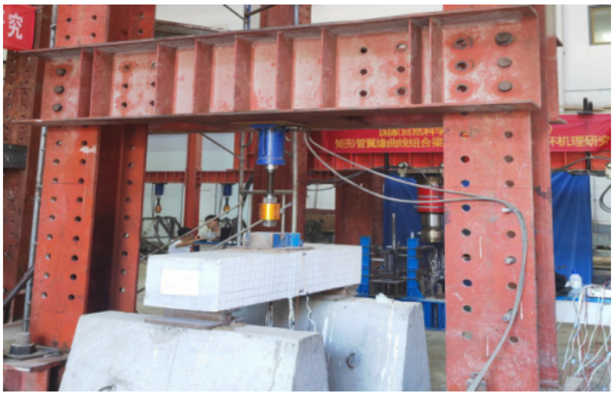

Figure 15. Testing Equipment.

According to Standard GB/T 50152-2012, the loading system is formulated. The main measure contents include the load sensor and TS-5A intelligent tester, which are used to record load sensor data during component loading. The mid-span displacement is measured using an SDP-100 displacement meter, and the load–deflection curve is drawn based on this. The width of the crack is observed and recorded by an integrated crack width meter. The strain of reinforcement and concrete is measured using the DH3816N-2 strain box and a computer.

4. Experimental Results and Discussion

4.1. Experimental Phenomena

1. Cast-in-place plate

Test phenomena and failure patterns of Specimen 1-1 are shown in Figure 16. At the initial stage of loading, the load increment of each stage is 5.23 kN. When the load is achieved at 41.75 kN, cracks occurr on Specimen 1-1, located at 79 cm, 80 cm, 85 cm, 84 cm, and 78 cm, respectively, from the left edge of the plate. This is because the tensile stresses in the concrete at the tensile edges of the section reach the ultimate strain of its tensile strength. The first cracks appear in the weakest tensile section of the member. With the increase in the load, the number of cracks in the middle part of Specimen 1-1 plate span increases gradually. When the load reaches 83.47 kN, a transverse crack of 2 cm appears 8 cm from the upper edge of the plate. When the load reaches 125.07 kN, a transverse crack of 5 cm appears 77 cm from the left edge of the plate and 5 cm from the upper edge. At this point, the width of the main crack reaches about 3 mm. A flexural crack 82 cm from the left edge of the plate develops almost to the whole height of the plate section. The load continues to increase and the crack height basically stops growing. However, the width continued to widen. Meanwhile, the displacement in the mid-span increases rapidly. Finally, the top crack develops horizontally. When the load reaches 140.7 kN, the reinforcement in the tension zone of the plate strip reaches yield strain. The concrete in the compression zone is crushed. Meanwhile, the crack width reaches about 5 mm. The deformation has a high possibility to continuously develop. In summary, the process of damage to the cast-in-place concrete plate is slow. Obvious signals can be detected before failure.

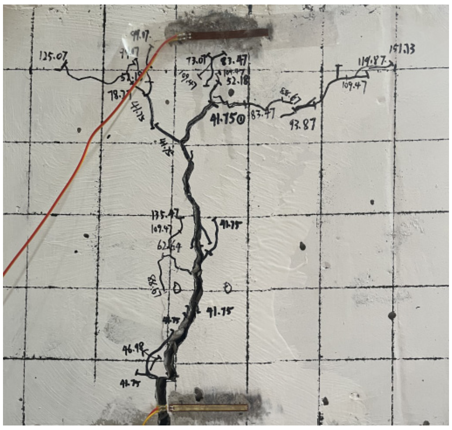

(a)

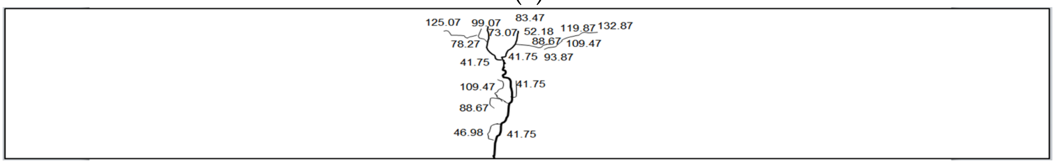

(b)

Figure 16. Experimental Phenomenon and Failure Mode of Cast-in-Place. (**a**) Topical of specimen 1-1; (**b**) Whole of specimen 1-1.

2. U-shaped steel connection

Test phenomenon and failure pattern of Specimen 2-3 are shown in Figure 17a. When the load is loaded in stages to 15.69 kN, two cracks at 70 cm and 100 cm away from the edge of the plate propagate. The reason for this is the difficulty in achieving the effect of one overall pouring at the interface of old and new concrete [25]. The bond strength at the interface is less than the tensile stress of the concrete, and the damage occurs earlier than the tensile damage of the concrete. Loading continues to increase to 62.64 kN and the vertical cracks continue to develop upwards. The maximum crack width increases to around 1.5 mm. When the load reaches 93.87 kN, a 2 cm long transverse crack appears. When the load reaches 132.87 kN, the crack width rapidly increases to about 10 mm. The concrete in the compressed area is crushed and the reinforcement yields. A slip occurs at the connection between U-shaped steel and transverse reinforcement. The load-bearing capacity decreases rapidly, the deflection increases, and the component is crushed. The test phenomenon and the failure pattern of Specimen 2-1 are shown in Figure 17b. When the load on Specimen 2-1 reaches 106.87 kN, the inclined crack extends to the top of the plate. At this point, two longer transverse cracks appear. This is due to the short lap length of the component U-shaped steel. The splitting failure and early damage occur along the reinforcement lap part [26].

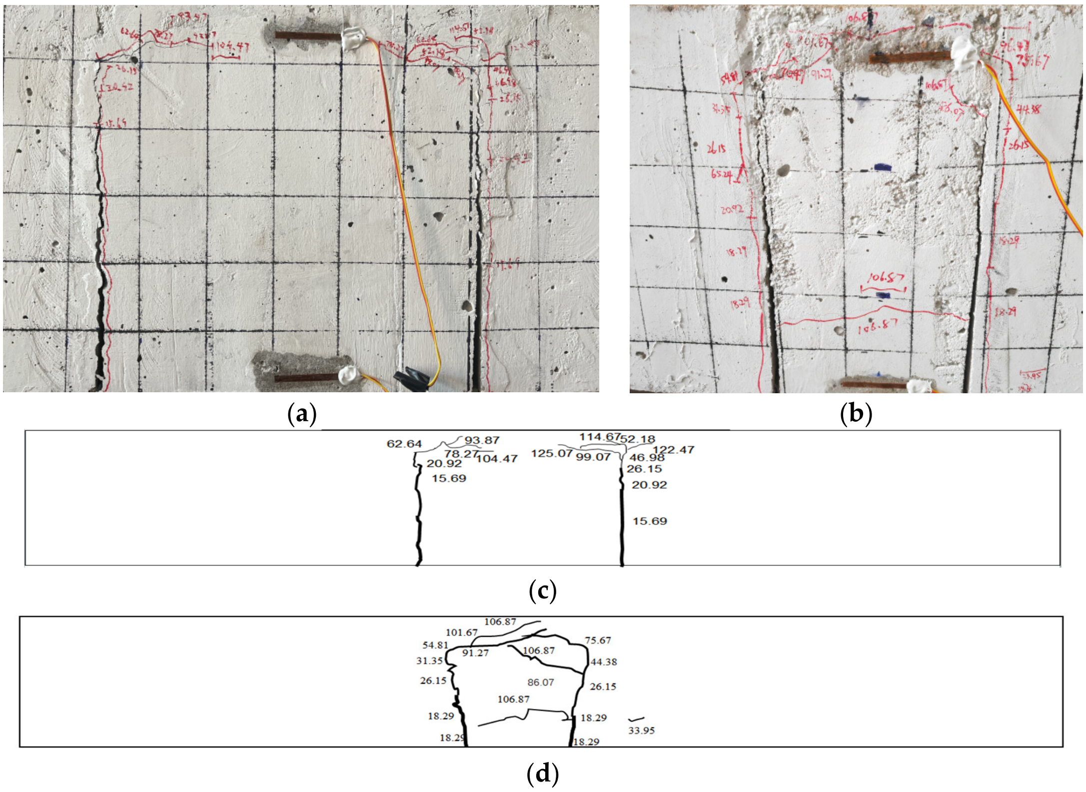

Figure 17. Experimental Phenomenon and Failure Mode of U-bar connection. (**a**) Topical of Specimen 2-3; (**b**) Topical of Specimen 2-1; (**c**) Whole of Specimen 2-3; (**d**) Whole of Specimen 2-1.

3. Lap connections

The test phenomenon and failure pattern of Specimen 3-1 are shown in Figure 18. When the load is 15.69 kN, the specimen develops two cracks located at the junction of the old and new concrete sections. When the load reaches 39.15 kN, the vertical crack continues to develop, and the crack width reaches about 3 mm. A 4 cm inclined crack appears as well. When the load reaches 73.07 kN, the inclined crack extends upward to the section height, 61 cm from the left edge of the plate. Its width increase to about 7.8 mm. At 106 cm from the left edge of the plate, the maximum crack width is about 24 mm. The steel bar in the tensile area yields and emits a “bang” sound. Lap reinforcement undergoes large slips due to unreliable connections. The deflection of the mid-span increases sharply. The specimen is recorded in a brittle failure mode.

4. Grouted Sleeve Connection

When the load is loaded to 39.15 kN, Specimen 4-1 begins to crack 97 cm from the edge of the plate. With the increase in load, the number of cracks in the middle span of Specimen 4-1 plate increases gradually. The vertical cracking continues to develop when the load reaches 52.18 kN. A 5 cm horizontal crack appears 97 cm from the left edge of the plate strip. When the load reaches 109.47 kN, a large number of cracks appear in the concrete compression zone. Meanwhile, the width of the main crack reaches about 6 mm. The upper part of the concrete begins to break up. When the load reaches 114.67 kN, the reinforcement in the tensile zone of the plate reaches yield strain. Meanwhile, the crack reaches a width of around 7 mm. At this point, the concrete in the compression zone is crushed and the reinforcement yields. The load-bearing capacity drops rapidly and the deflection increases continuously. The test phenomenon and failure pattern are shown in Figure 19.

(**a**)

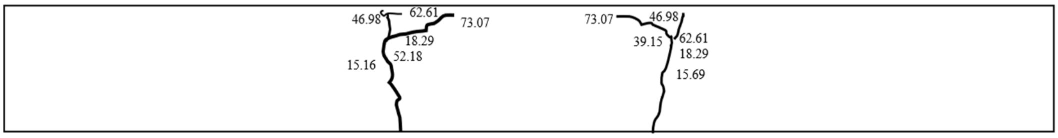

(**b**)

Figure 18. Experimental Phenomenon and Failure Mode of lap connections. (**a**) Topical of Specimen 3-1; (**b**) Whole of Specimen 3-1.

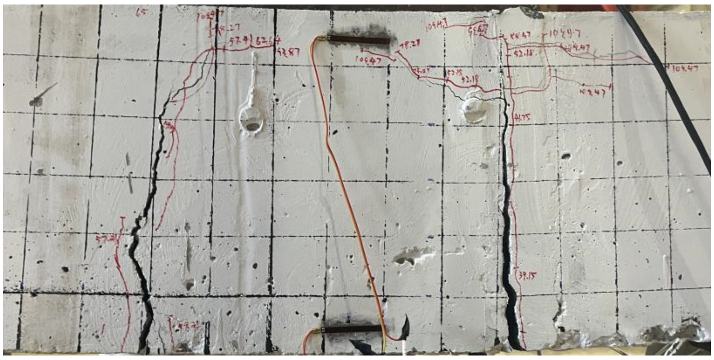

(**a**)

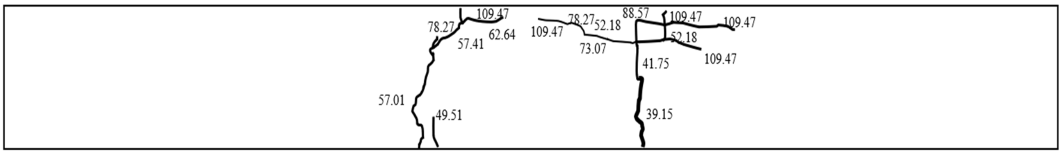

(**b**)

Figure 19. Experimental Phenomenon and Failure Mode of Grouted Sleeve Connection. (**a**) Topical of Specimen 4-1; (**b**) Whole of Specimen 4-2.

4.2. Analyses and Discussions

4.2.1. Load-Mid-Span Deflection Analysis

Deformation performance is an important indicator to determine whether the component meets the serviceability limit state. During the test, the vertical deformation data of the plate in the loading process were collected by the dial indicator. The recorded mid-span vertical displacement value and the corresponding test load were drawn into the load-mid-span deflection curve. According to the graph, the influence of the prefabrication connection mode and the length of the steel lap on the deformation performance was analyzed.

For Specimen 1-1, when the load was increased to 140.7 kN, the ultimate load recorded for the test was reached. For Specimens 2-1, 2-2, 2-3, 2-4, 2-5, and 2-6, the ultimate load of the test record was reached when loaded to 106.87 kN, 127.67 kN, 132.87 kN, 132.87 kN, 130.27 kN and 125.07 kN, respectively. The ultimate load of each specimen reached 76%, 90.7%, 94.4%, 94.4%, 92.6%, and 88.9% of the ultimate load of cast-in-place structure, respectively, indicating that the U-shaped steel connecting prefabricated plate foundation has high bending bearing capacity. Specimen 3-1 reached the ultimate load when loaded to 73.07 kN. Compared with the cast-in-place concrete plate strip, the ultimate bearing capacity was lower. The ultimate bearing capacity of Specimen 4-1 was 114.67 kN, reaching 81.5% of the ultimate load of the cast-in-place component, and the mechanical properties of the material were fully utilized.

According to the provisions of the Code for Design of Concrete Structures GB 50010, the maximum allowable deflection of the specimen is 7 mm. Specimens 1-1, 2-1, 2-2, 2-3, 2-4, 2-5, 2-6, 3-1, and 4-1 reached the maximum allowable deflection at 54 kN, 42 kN, 40 kN, 45 kN, 56 kN, 40 kN, 46 kN, 45 kN, and 56 kN, respectively. Compared with specimen 1-1, when the load reached 54 kN, the mid-span deflection of Specimen 2-1 increased by 2.9 mm, while the deflection of Specimen 2-3 increased by 2 mm, and that of Specimen 3-1 increased by 1.5 mm. This is because the prefabricated plate foundation after the cast of concrete and the original concrete connection interface are weak [27], increasing the mid-span deflection.

The load-mid-span deflection curve of each specimen is shown in Figure 20. At the beginning of loading, the change curves of different specimen plates basically coincide with each other. The way the prefabricated members are connected has less effect on the cracking loads as well as the stiffness of the members. Specimens 2-1, 2-2, and 2-3 are three U-shaped steel specimens with different lap lengths, and the comparison curves of the three are shown in Figure 20a. From Figure 20a, it can be seen that the ultimate load on the component increases as the lap length of the U-shaped steel increases. The deflection in the mid-span of Specimen 2-2 is higher when the load is kept the same. The comparison curves for Specimens 2-1, 2-3, and 2-4 with different post-cast materials are shown in Figure 20b. From Figure 20b, it can be seen that the ultimate loads of Specimens 2-3 and Specimens 2-4 are approximately 1.24 times higher than those of Specimen 2-1. This is due to the larger anchorage length of the U-shaped steel in Specimen 2-3. The post-cast section of Specimen 2-4 was made with a high-strength grout, which has high compressive strength. In Specimen 2-1 and Specimen 2-3, the reduced length of the lap connection can play a role in hindering the development of cracks. The small difference in vertical displacement between Specimen 2-3 and Specimen 2-4 at the time of damage is due to the high-strength grout used in the post-cast part of Specimen 2-4, which has high compressive strength and high overall stiffness. The comparison curves of four different connection schemes of Specimens 1-1, 2-3, 3-1, and 4-1 are shown in Figure 20c. It is known from Figure 20c that the limit load of Specimens 2-3 is about twice that of Specimens 3-1, so the connection of U-shaped steel is more reliable than that of steel lap. The vertical deformation of Specimens 2-3 and 3-1 is basically the same, so the ductility is not much different. Specimen 4-1 has less vertical displacement than Specimen 1-1. This is due to the high reliability of grouted sleeve connections. The comparison curves of Specimens 1-1, 2-1, 2-2, 2-3, 2-4, 2-5, 2-6, 3-1, and 4-1 are shown in Figure 20d. As shown in Figure 20d, the vertical deformation of the prefabricated foundation plate strip is always greater than that of the cast-in-place concrete plate strip. This is because the deformation capacity of the plate strip is significantly enhanced by the lap connection of the rebar in the post-cast strip [28–30]. The ultimate load of Specimen 2-6 is approximately 1.2 times that of Specimen 2-1. Its anchorage length was obtained according to a reinforcement strength of 100 MPa. This shows that the bearing capacity of Specimen 2-6 meets the requirements.

During the loading process, the load-mid-span deflection curve of the prefabricated specimen is similar to that of Specimen 1-1 and is divided into three typical stages. The initial stage is the linear elastic stage. When the concrete surface cracks and the number of cracks gradually increases, the stiffness of the specimen decreases. The change speed of vertical deformation is greater than that of the load change. This stage is the crack development stage. In the third stage, the tensile reinforcement of the specimen yields, and the rate of change in deflection is accelerated. This is the same pattern of change as for ordinary concrete plates and strips [31].

4.2.2. Calculation of Flexural Capacity

In this study, the anchoring of longitudinal reinforcement of precast members in post-cast concrete complies with the provisions of the current national standard Code for Design of Concrete Structures GB 50010 and Technical Specification for Application of Headed Bars JGJ 256 [32]. According to the provisions of Article 6.2.10 of the Code for Design of Concrete Structures (GB 50010-2010) [21], the flexural bearing capacity of the load–deflection curve of each specimen is calculayed, as shown in Formulas (2) and (3).

$$M \leq M_u = \alpha_1 f_c b x \left(h_0 - \frac{x}{2}\right) + f'_y A'_s \left(h_0 - a'_s\right). \tag{2}$$

The height of the concrete compression area is determined according to the following formula:

$$\alpha_1 f_c b x = f_y A_s - f'_y A'_s, \tag{3}$$

where M is the design value of the bending moment; M_u is the bending moment that the section can resist; the coefficient α_1 is calculated according to Article 6.2.6 of the specification, 1.0. The f_c and $f_y{}'$ are the axial compressive strength of concrete and the tensile strength of rebar, respectively. The $f_y{}'$ takes the steel material test results in Table 3. The f_c takes the axial compression strength of concrete test results in Table 3. A_s and $A_s{}'$ are the section area of the longitudinal reinforcement in the tensile area and the compression area, respectively. b is the width of the rectangular section. x is the depth of the compression zone; h_0 is the effective depth of section. a'_s is the distance between the joint point of ordinary longitudinal reinforcement in the compression area to the edge of the compression section.

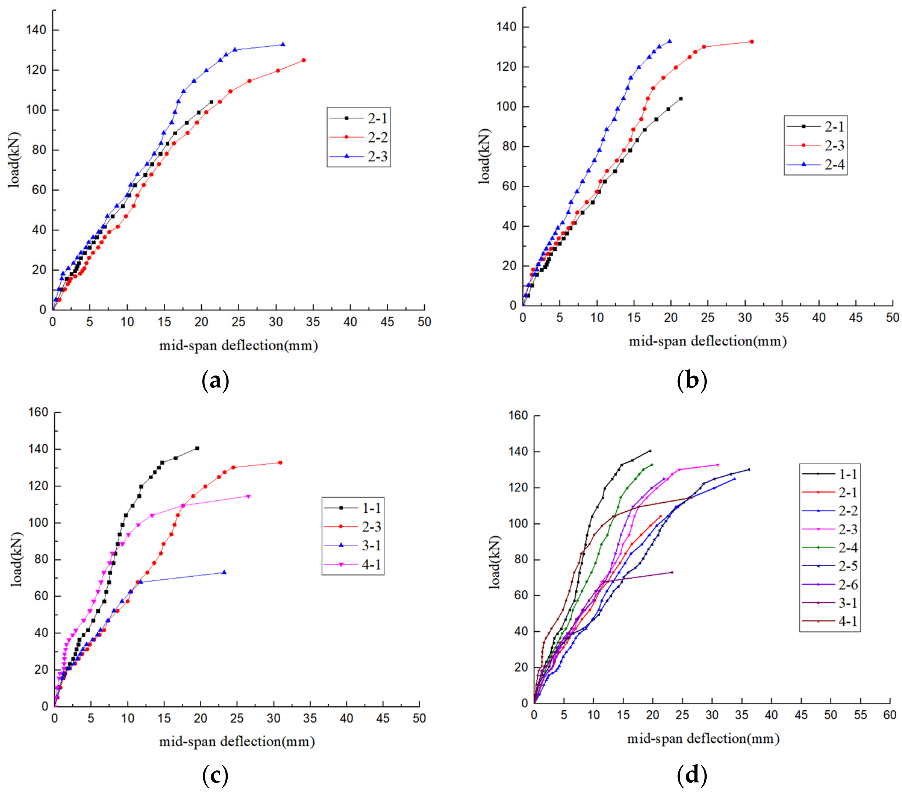

(**a**) (**b**) (**c**) (**d**)

Figure 20. Relationship between Load and Mid-Span Deflection. (**a**) Different lap length; (**b**) Different post-pouring materials; (**c**) Different splicing schemes; (**d**) Scheme summary.

The comparison results of calculated and test values of flexural bearing capacity are shown in Table 7. Except for Specimen 3-1, the error of the other specimens is between 8.9% and 15.3%. It shows that the calculation formula of flexural bearing capacity in the current specification is suitable for the calculation of the flexural bearing capacity of the specimen. The flexural load capacity formula in the above-referenced Code for Design of Concrete Structures does not take into account the tensile effect of the reinforcement in the compression zone of the plate, and the compressive effect of concrete can increase the flexural load capacity. Therefore, the test value of the flexural bearing capacity of the plate is greater than the calculated value.

The flexural bearing capacity was increased, as the anchorage length of the prefabricated U-shaped steel connecting plate was extended. The flexural bearing capacity test value of Specimen 2-1 is slightly less than the calculated value. This is due to the small lap length causing splitting damage to the specimen. The remaining prefabricated specimen test value is larger than expected. This also shows that the prefabricated plate strip has a certain safety reserve [33]. Specimen 3-1 has a large error between the test value and the calculation value, and it is less than the calculated value obtained by the gauge formula. This is due to the low anchorage strength of the reinforcement in the lap connection scheme, which leads to fragility damage occurring in the prefabricated plate strip.

Table 7. Comparison of Tested Bending Capacity and Code-based Value.

Specimen Number	Experimental Value/(kN·m)	Theoretical Value/(kN·m)	Experimental Value/Theoretical Value
1-1	38.69	33.54	1.15
2-1	29.39		0.88
2-2	35.10		1.05
2-3	36.54		1.09
2-4	36.54		1.09
2-5	35.82		1.07
2-6	34.39		1.03
3-1	20.09		0.60
4-1	31.53		0.94

4.3. Finite Element Simulation Analysis

The mechanical behavior of the designed prefabricated plate foundation plate strip is simulated using the ABAQUS finite element software. By analyzing the stress distribution of the components, the mechanical properties of the plate and strip in the design example are verified to provide support for the prefabricated plate foundation design method.

4.3.1. Modelling

Numerical simulations on Specimen 1-1, Specimen 2-3, and Specimen 2-4 were conducted. The prefabricated foundation plate and strip model are composed of concrete and reinforcement stages. The tensioned bar adopts HPB300-grade reinforcement. Elastic and plastic models [34] were used for tensioned bars and plastic damage models for C30 concrete. Material properties adopt test-measured value. Concrete adopts the C3D8R solid element. The grid was divided into regular hexahedral elements. The reinforced steel bar adopted a T3D2 truss unit. The unit length was 40 mm, embedded in contact with concrete. The binding was set between the later-poured concrete and the first-poured concrete [35]. Frictional contact was provided between the steel plate and the plate and strip. The finite element model is shown in Figure 21. Details of the number of nodes and cells in each model are shown in Table 8 below.

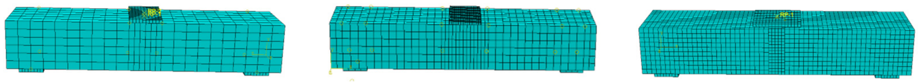

(**a**) (**b**) (**c**)

Figure 21. Finite Element Model. (**a**) Test Specimen 1-1; (**b**) Test Specimen 2-3; (**c**) Test Specimen 2-4.

Table 8. Details of the number of nodes and elements.

Specimen Number	Number of Nodes	Number of Elements
1-1	2791	1732
2-3	10,872	6156
2-4	15,373	9751

4.3.2. Foundation Boundary Conditions and the Loading Protocol

To accurately simulate the plate and strip force, the model applied 1172.5 kN/m^2 and 1107.25 kN/m^2, 1476.3 kN/m^2 on the steel plate on the upper surface. The loading process was completed in a nonlinear smoothing mode. A constraint was imposed at the point where the bottom meets the backing plate to limit the displacement and angle [36].

4.3.3. Stress Analysis

The stress cloud map of plate and strip concrete is shown in Figure 22. It can be seen from Figure 22 that the stresses in the specimen at the time of damage are mainly concentrated in the area of the compression bending section. The concrete stresses in the compression-bending section reach the maximum, indicating that the plate zone eventually cracks along the mid-span and at the interface between the old and new concrete, which is consistent with the test phenomenon. The stress cloud for the reinforcement in the plate is shown in Figure 23. It can be seen from Figure 23 that the steel stress on the tensile side of Specimen 1-1 is significantly greater than the steel stress on the compression side. The maximum steel stress of Specimens 2-3 and 2-4 is small compared with that of Specimen 1-1. This is because the compressive side of the U-shaped steel can share the tensile stress with the tensile side. Therefore, Specimen 2-3 exerts higher stress on the compressed side of the reinforcement. The high-strength grout in the post-cast portion of Specimen 2-4 can carry the load together with the reinforcement. Therefore, the stresses in the reinforcement on the compressive side are lower. In summary, the U-shaped steel connection method is significantly different from ordinary reinforcement in cast-in-place plates in terms of stress transfer path and distribution.

The simulation results of the displacement cloud map of each specimen are shown in Figure 24. The three specimens are a typical flexural failure, and the span deflection is consistent with the test results. Figure 24 shows the comparison results of the load-mid-span medium deflection simulation value and the measured test value of Specimens 1-1, 2-3 and 2-4. As can be seen from Figure 24, the finite element simulation results agree well with the measured test value. The overall error is small, so the flexural performance of each specimen can be simulated more accurately.

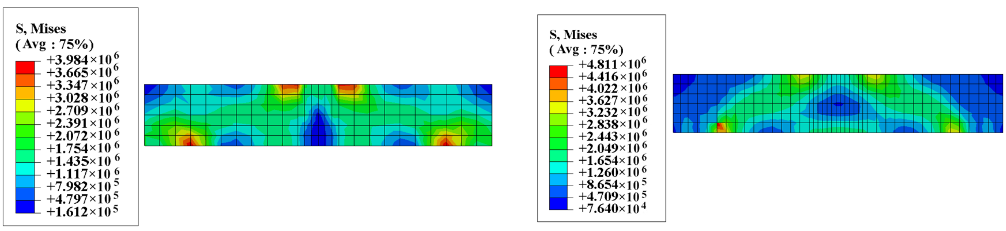

(**a**) (**b**)

Figure 22. *Cont.*

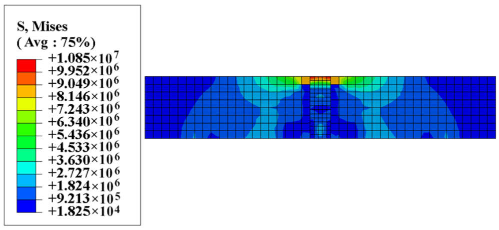

(**c**)

Figure 22. Concrete Stress Cloud Diagram of Plate and Strip. (**a**) Test Specimen 1-1; (**b**) Test Specimen 2-3; (**c**) Test Specimen 2-4.

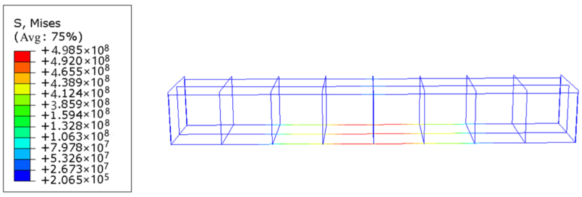

(**a**)

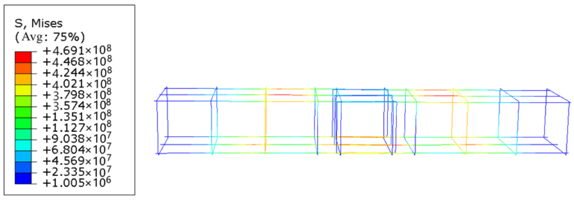

(**b**)

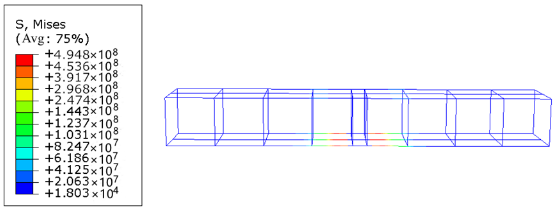

(**c**)

Figure 23. Reinforcement Stress Cloud Diagram of Plate and Strip. (**a**) Test Specimen 1-1; (**b**) Test Specimen 2-3; (**c**) Test Specimen 2-4.

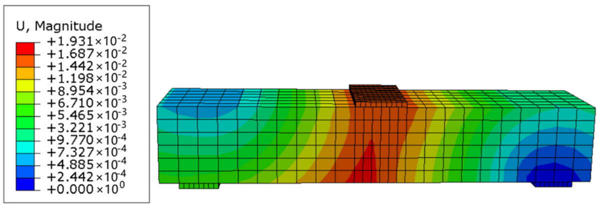

(**a**)

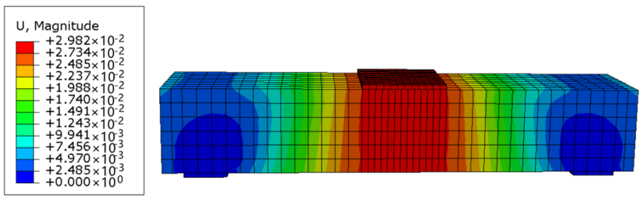

(**b**)

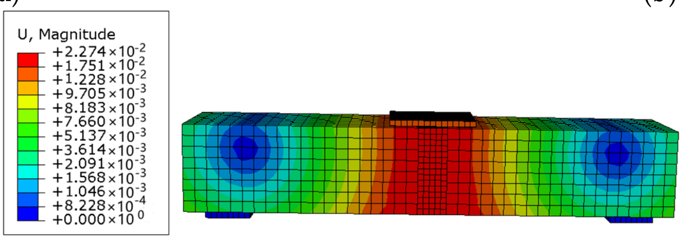

(**c**)

Figure 24. Displacement Cloud Diagram of Plate and Strip. (**a**) Test Specimen 1-1; (**b**) Test Specimen 2-3; (**c**) Test Specimen 2-4.

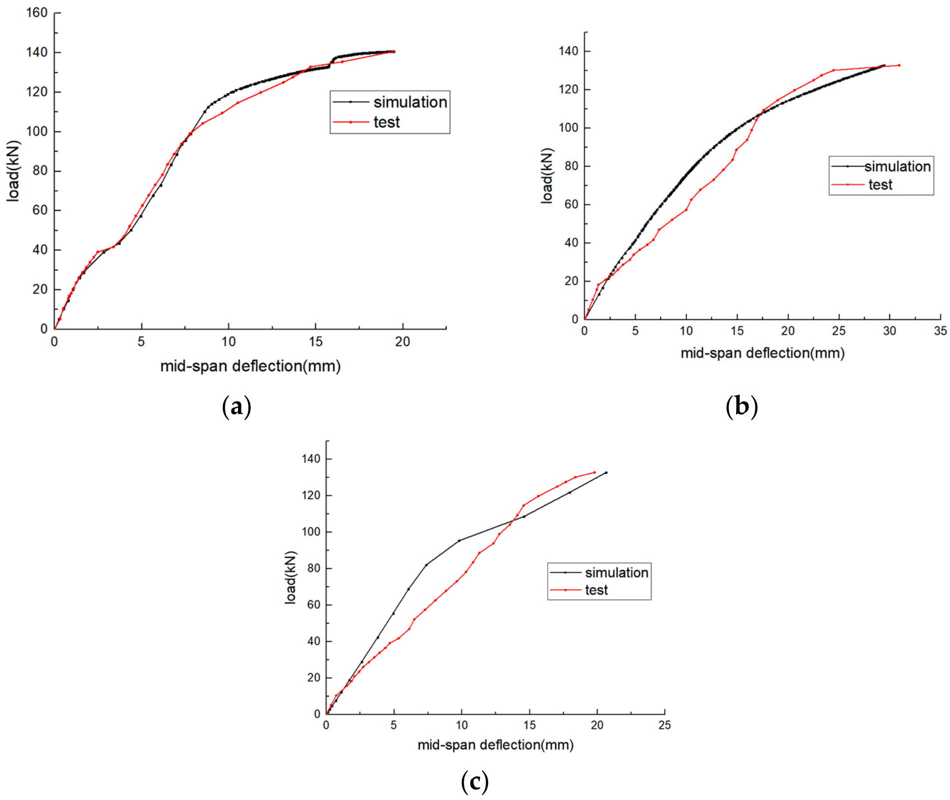

Figure 24. Comparison between Simulated and Measured Mid Span Deflection of Plate and Strip. (**a**) Test Specimen 1-1; (**b**) Test Specimen 2-3; (**c**) Test Specimen 2-4.

5. Conclusions

The schemes of post-pouring belt U-shaped steel connection, post-pouring belt lap connection, grouting sleeve connection, and post-tensioned bond prestressed reinforcement connection were newly proposed to apply on plate foundation with the purpose of improving green and intelligent construction technology for tower foundations, shortening construction time, and reducing labor force. Different plate splicing schemes were compared in view of component processing, transporting, on-site constructing, and performance. Furthermore, pseudo-static tests were conducted to study its basic mechanical behavior. The following conclusions were obtained:

1. The post-cast belt U-shaped steel connection is recommended with the advantages of low processing difficulty and high reliability. The flexural load-bearing capacity of spliced plates with the scheme of post-pouring belt lap connection is much lower than that of cast-in-place plates. Grouted sleeve connections and prestressing tendon connection schemes have complex processing and difficult construction and are not recommended.
2. The typical flexural failure of a U-shaped steel connecting strip is basically the same as that of an ordinary concrete plate belt. The flexural load-bearing capacity of the U-shaped steel connecting plate can reach more than that of 90% of the cast-in-place member, which is basically equivalent to the values of cast-in-place members. The ductility coefficient ratio of prefabrication nodes to cast-in-place nodes is about 1.5, with increased ductility.
3. The load-bearing capacity of the component is relevant to the anchorage length of the U-shaped steel. Splitting failure along the lap reinforcement may occur if the lap splice length of the U-shaped steel is not sufficient. However, the load-bearing capacity still meets the code requirements when the anchorage length is 0.3 *la*.
4. Compared to the fact that most flexural cracks of the cast-in-place specimens were located in the pure bending span, the concrete damage of prefabricated specimens

in the spliced region and the pure bending span were more serious. Improving the strength grade of concrete can promote the ultimate bearing capacity of the prefabricated concrete plate and strip connecting joints. The high-strength grouting material used in the design can greatly shorten the construction period, which has obvious advantages for a project with a tight construction period.

5. The prefabricated plate foundation for transmission towers has a good application prospect. However, its seismic resistance, corrosion resistance, and susceptibility to cracking need to be further studied.

Author Contributions: Writing—original draft, W.W., Y.G. and Z.W.; project administration, L.Z., Z.A. and S.S. All authors have read and agreed to the published version of the manuscript.

Funding: This research work was jointly supported by the National Natural Science Foundation of China (Grant No. 51908340) and the financial support from Major Scientific and Technological Innovation Project of Shandong Province (Grant No. 2021CXGC011204).

Data Availability Statement: Not applicable.

Conflicts of Interest: The authors declare no conflict of interest.

References

1. Akbari, G.A.; Armin, S.K. Ultimate Bearing Capacity of Helical Piles as Electric Transmission Tower Foundations in Unsaturated Soils: Analytical, Numerical, and Experimental Investigations. *Int. J. Geomech.* **2022**, *22*, 04022194.
2. Ding, S.; Cheng, Y.; Zheng, H.; Xue, F.; Nie, Z.; Man, Y. Uplift Bearing Capacity of Transmission Tower Foundation in Reinforced Aeolian Sand Using Simplified Model Tests. *Adv. Civ. Eng.* **2021**, *2021*, 6630731. [CrossRef]
3. Rattley, M.J.; Richards, D.J.; Lehane, B.M. Uplift Performance of Transmission Tower Foundations Embedded in Clay. *J. Geotech. Geoenvironmental Eng.* **2008**, *134*, 531–540. [CrossRef]
4. Peng, B.; Wang, X.Y.; Wang, Y.; Huang, H. Geometry Optimization and Engineering Applications of Transmission Tower Foundation in the Slope. *Appl. Mech. Mater.* **2013**, *2746*, 1243–1247. [CrossRef]
5. Li, W.; Li, Y.; Shang, J.; Chen, Y.; Zu, J. Research on the Durability of Composite Pile Made of Ultra-High-Performance and Common Concrete: Finite Element Analysis. *IOP Conf. Ser. Earth Environ. Sci.* **2021**, *719*, 022072. [CrossRef]
6. Yuan, G.; Yang, B.; Huang, Z.; Tan, X. Experimental study on the stability of the transmission tower with hybrid slab foundation. *Eng. Struct.* **2018**, *162*, 151–165. [CrossRef]
7. Zhou, Y.; Chen, H.; Zhou, Q.; Duan, Z.; Gao, X. Determination of Ultimate Load and Stability Evaluation of Transmission Tower Foundation during Operation Period. *J. Phys. Conf. Ser.* **2020**, *1654*, 012122.
8. Xie, X.; Wang, D.; Qian, Y.; Jin, Y. Summary of Research Status of Assembly Nodes. *IOP Conf. Ser. Earth Environ. Sci.* **2019**, *330*, 022072. [CrossRef]
9. Qiu, T.; Zhang, J.; Chen, X.; Xu, Z.; Su, D.; Song, R.; Cui, T. Experimental investigation and mechanical model for assembled joints of prefabricated two-wall-in-one diaphragm walls. *Eng. Struct.* **2023**, *275*, 115285. [CrossRef]
10. Li, S.; Lu, W.; Sun, H.; Luan, Y. Experimental and numerical research on fabricated joint for CFST set in underground construction. *Structures* **2021**, *34*, 1291–1299. [CrossRef]
11. Liu, D.; Fu, Q.; Wang, J.; Wang, M.; Li, W.; Liu, M. Study on recyclable precast-slab-fabricated road based on arching effect theory. *Eng. Res. Express* **2022**, *4*, 045019. [CrossRef]
12. Huang, Y.; Wu, Q.; Tang, T. Seismic Performance and Design of the Fully Assembled Precast Concrete Frame with Buckling-Restrained Braces. *Buildings* **2022**, *12*, 1818. [CrossRef]
13. Ye, J.; Yan, G.; Liu, R.; Xue, P.; Wang, D. Hysteretic behavior of replaceable steel plate damper for prefabricated joint with earthquake resilience. *J. Build. Eng.* **2022**, *46*, 103714. [CrossRef]
14. Wang, S.; Xu, W.; Huang, X.; Yan, X.; Ma, J.; Sun, H.; Wang, J.; Chen, Y. Research on the Pounding Response and Pounding Effect of a Continuous Rigid-Frame Bridge with Fabricated Super-High Piers Connected by Grouting Sleeves. *Sustainability* **2022**, *14*, 11334. [CrossRef]
15. Baghdadi, A.; Heristchian, M.; Ledderose, L.; Kloft, H. Experimental and numerical assessment of new precast concrete connections under bending loads. *Eng. Struct.* **2020**, *212*, 110456. [CrossRef]
16. Chen, Y.; Lu, D.; Zhang, M.; Xie, G. Study on the connection properties of U-type reinforcement ring buckle of prefabricated concrete beam and column nodes. *J. Guangxi Univ. (Nat. Sci. Ed.)* **2019**, *44*, 1552–1561.
17. Lu, L.; Gao, M.; Guo, Y.; Wang, W.; Yan, H.; Jiang, T. Experiments on flexural behavior of the prefabricated RAC and NWC composite slab. *Ain Shams Eng. J.* **2022**, *13*, 101789. [CrossRef]
18. Liu, X.-C.; Song, J.; Chen, X.-S.; Qiang, S. Experimental study on prefabricated steel-reinforced concrete slab with C-type steel border. *Eng. Mech.* **2022**, *39*, 312–319.

19. Zhu, H. Test of Integral Frame Structure (Structure System of Precast Prestressed Concrete Assembly). Ph.D. Thesis, Southeast University, Nanjing, China, 2006.
20. Guo, L.; Zhang, Z.; Wang, X.; Yu, Q.; You, Y.; Yuan, C.; Xie, Y.; Gou, T. Stability analysis of transmission tower foundations in permafrost equipped with thermosiphons and vegetation cover on the Qinghai-Tibet Plateau. *Int. J. Heat Mass Transf.* **2018**, *121*, 367–376. [CrossRef]
21. Kong, W.; Li, M.; Xu, X. *Scheme Research of Assembly Type Steel Structure Transmission Tower Foundation*; Information Engineering Research Institute: Texas City, TX, USA, 2015; Volume 4.
22. *GB 50010-2010*; Code for Design of Concrete Structures. China Architecture & Building Press: Beijing, China, 2010.
23. *GB/T 50152-2012*; Standard for Test Method of Concrete Structures. China Architecture & Building Press: Beijing, China, 2012.
24. *GB/T50081-2002*; Standard for Test Method of Mechanical Properties on Ordinary Concrete. China Architecture & Building Press: Beijing, China, 2007.
25. Hu, Y.; Li, Z.; He, J.; Huang, Z. Experimental Study on Seismic Performance of Prefabricated Joints of Underground Utility Tunnel. *IOP Conf. Ser. Earth Environ. Sci.* **2019**, *267*, 042109. [CrossRef]
26. Yi, W.; Liu, C. Experimental study on the bending performance of the reinforced reinforced concrete beam. *J. Hunan Univ. (Nat. Sci.)* **2023**, *50*, 1–10.
27. Qian, H.; Zhu, Y.Y.; Zhang, Y.; Li, Z.; Zhao, J. Study on seismic performance of functional self-recovery prefabricated beam-column nodes. *China Civ. Eng. J.* **2023**, *56*, 57–65.
28. Liu, Y.L.; Liu, C.; Pan, H.; Fu, J.-L.; Huang, J.-Q.; Hong, J.-Q. Experimental and numerical investigation on seismic performance of semi-precast concrete sandwich shear wall. *Adv. Struct. Eng.* **2022**, *25*, 2772–2784. [CrossRef]
29. Pul, S.; Hüsem, M.; Arslan, M.E.; Hamzacebi, S. An experimental study on different socket base connections under cyclic loading. *Comput. Concr.* **2014**, *13*, 377–387. [CrossRef]
30. Zhou, X.; Wang, X.; Gu, C.; Chung, K.-F.; Liu, J.; Liao, Y.; Chen, X. Seismic behavior of a novel prefabricated thin-walled CFST double-column pier system for simple on-site assembly. *Thin-Walled Struct.* **2023**, *183*, 110388. [CrossRef]
31. Li, S.; Li, R.R.; Li, X.; Wang, Z. Study on quasi-static test of prefabricated beam and column nodes connected with cantilever section. *Earthq. Eng. Eng. Dyn.* **2022**, *42*, 239–249.
32. *JGJ 256-2011*; Technical Specification for Application of Headed Bars. China Architecture & Building Press: Beijing, China, 2011.
33. Lv, X.; Yu, Z.; Shan, Z. Seismic behaviour of frame structures with assembly of prefabricated concrete beam. *J. Build. Eng.* **2021**, *40*, 102765. [CrossRef]
34. Li, B.; Jian, M.J.; Zhang, D.Q.; Zhang, G.C. Finite Element Analysis of Foundation Settlement of 220kV Transmission Tower with Independent Foundation. *Appl. Mech. Mater.* **2012**, *1968*, 602–607. [CrossRef]
35. Li, S.; Xu, T.; Ding, S.; Li, X.; Guo, H.; Liu, Y. Seismic performance of a new assembled beam-column joint with cantilever beam splicing. *J. Constr. Steel Res.* **2022**, *196*, 107432. [CrossRef]
36. Xu, F.; Xie, K.; Xu, W. Finite element analysis of static performance of new fabricated double-layer upper flange composite beam. *J. Phys. Conf. Ser.* **2022**, *2202*, 012011. [CrossRef]